Autowaves and Spatio-Temporal Chaos in CNNs—Part I: A Tutorial

Ladislav Pivka

Abstract—**This paper presents a summary of the most commonly observed spatio-temporal phenomena in discrete cellular neural networks (CNNs) of dimension one and two. Among the phenomena discussed are traveling wave phenomena in chains and 2-D arrays, and spiral waves and target waves in both excitable and fluctuating media. Chua's circuit is used as the basic cell in the CNN arrays. Parameter values and initial conditions for the corresponding simulations are given so they can be reproduced with different simulators.**

I. Introduction

AUTOWAVES and especially spiral waves are the most frequently encountered wave phenomena in the study of natural phenomena in biology, chemistry, and physics [1]–[3]. While traveling waves can arise in discrete media in which each elementary cell is excitable or bistable, spiral waves and scroll waves—3-D analogs of spiral waves—can develop in either excitable [4], fluctuating [5], or even chaotic media [6]. We will explain briefly the notions of excitable, fluctuating, and chaotic media. The global behavior of a discrete medium depends on the dynamics of its constituent parts—neurons, and the type of interconnections between them. Since Chua's circuit [7] can exhibit a wide variety of dynamic behaviors we can use it conveniently as a building block for any of the above-mentioned type of media.

Excitable medium is one in which each individual neuron (Chua's circuit) exhibits one stable state (*rest* state). Under excitation or forcing (which can be provided by the neighboring cells via coupling, or externally) the cell "fires," i.e., one or more of its variables change their values dramatically (*excitation* state). A period of *relaxation* follows with a slow change in the variables, after which the system recovers quickly in the *refractory* period, and is ready to fire again.

In a *fluctuating*, nonexcitable, discrete medium each neuron operates in a stable periodic regime (i.e., each cell exhibits only one stable limit cycle), whereas in a *chaotic* medium the regime of each cell is chaotic (corresponding to a chaotic attractor).

In addition to the above discrete media we will consider media represented by bistable cells (i.e., there are two point attractors for each cell), used in the generation of traveling waves.

Manuscript received January 10, 1995; revised May 15, 1995. This work was supported in part by the Office of Naval Research under Grant N00014-89-J-1402 and the National Science Foundation under Grant MIP 86-14000. This paper was recommended by Guest Editor L. O. Chua.

The author is with the Electronics Research Laboratory and Department of Electrical Engineering and Computer Sciences, University of California, Berkeley, CA 94720 USA.

IEEE Log Number 9414459.

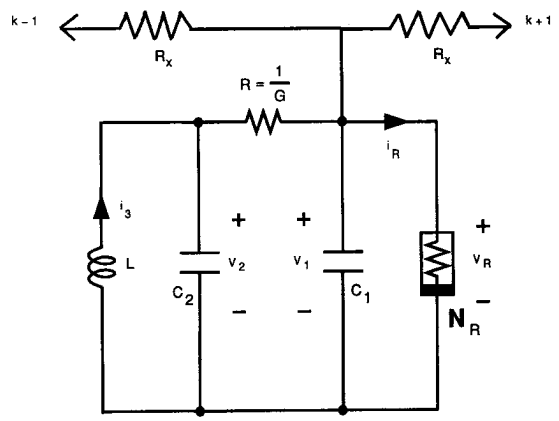

Fig. 1. Schematic diagram of a one-dimensional array of resistively coupled Chua's circuits.

II. Traveling Wave Phenomenon

Transport processes in living tissues, chemical, and physiological systems have been found to be associated with a special type of autowaves called traveling waves [8]–[10]. Earlier, continuous models were created to describe such phenomena, but failed to cover all important aspects of the traveling wave behavior. One of the most important of them is the so-called traveling wave propagation failure, occurring at weak coupling between cells. It has been proved by Keener [11] that propagation failure cannot be observed in a continuous, one-variable, homogeneous reaction-diffusion system. Therefore, in studying those phenomena we must use discrete models. Traveling waves and propagation failure in arrays of Chua's circuits have been studied in [12]. Here we reproduce those phenomena and give an intuitive explanation of the underlying triggering processes by using numerical simulations.

A. Traveling Waves in Chains of Chua's Circuits

Fig. 1 shows a schematic representation of a chain of resistively coupled Chua's circuits. The dynamics of the chain is governed by the following system of equations

$$\begin{aligned} \dot{x}_k &= \alpha(y_k - f(x_k)) + D(x_{k-1} - 2x_k + x_{k+1}) \\ \dot{y}_k &= x_k - y_k + z_k \quad (k = 1, \cdots, l) \\ \dot{z}_k &= -\beta y_k \end{aligned} \tag{1}$$

where

$$\begin{aligned} f(x) = (1/2)[&(s_1 + s_2)x + (s_0 - s_1)(|x - B_1| - |B_1|) \\ &+ (s_2 - s_0)(|x - B_2| - |B_2|)] + \epsilon \end{aligned} \tag{2}$$

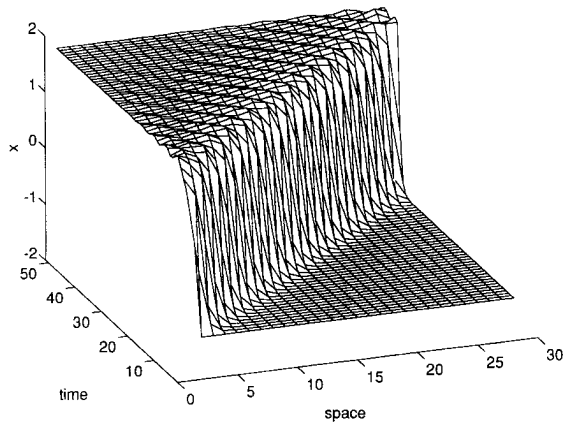

Fig. 2. Traveling wavefront in a chain of 28 Chua's circuits, with diffusion coefficient $D = 0.6$. The wave propagation was initiated by setting cell 1 to equilibrium point $\mathbf{P}^+$. After about 50 time units all cells have switched to $\mathbf{P}^+$.

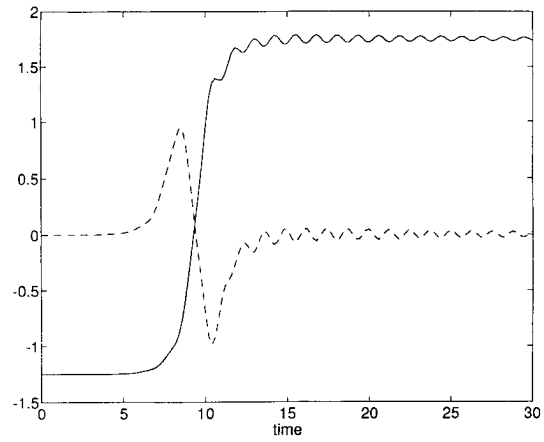

Fig. 3. Time waveforms of the diffusion term $D(x_{k-1} - 2x_k + x_{k+1})$ (dashed line) and variable x (solid line) in cell 5 of the chain in Fig. 2.

is a three-segment piecewise-linear function with breakpoints $B_1 = -1$ and $B_2 = 1$, α and β are appropriately scaled circuit parameters, $D = \alpha/(GR)$ is the diffusion coefficient, and l is the chain length. To obtain bistable cells, parameter values were chosen as follows [13]:

$$\alpha = 9, \quad \beta = 30, \quad s_1 = s_2 = 2/7,$$
$$s_0 = -1/7, \quad \epsilon = -1/14 \tag{3}$$

where s_0, s_1, s_2 are the slopes of the middle, left-hand, and right-hand segment, respectively.

For a traveling wave to arise with a symmetric choice of slopes s_1 and s_2 it is necessary to include an offset $\epsilon \neq 0$ in the function f: $\epsilon = -1/14$, according to [13]. Another possibility would be to use an asymmmetric function f, e.g., with $s_0 = -1/7$, $s_1 = 2/7$, $s_2 = 1/7$ and zero offset ϵ. Zero flux (Neumann) boundary conditions were used in our numerical computations, which in this context means setting $x_0 = x_1$ and $x_{l+1} = x_l$ at each integration step; similarly for variables y and z.

The above choice of parameter values (3) guarantees the existence of two stable equilibrium points $\mathbf{P}^- = [-1.25, 0, 1.25]$,$\mathbf{P}^+ = [1.75, 0, -1.75]$ for each cell, corresponding to segments s_1 and s_2, respectively. Due to an asymmetry in function f, the basin of attraction of the point $\mathbf{P}^+$ is much larger than that of $\mathbf{P}^-$ and, loosely speaking, it is harder to steer a trajectory back into the basin of $\mathbf{P}^-$ once it is in the basin of $\mathbf{P}^+$.

Propagation of a traveling wave in the chain depends on a triggering mechanism which we describe briefly. A similar triggering mechanism for a tristable Chua's circuit has been described in [15].

Consider a single cell and assume, for example, that the initial state is in point $\mathbf{P}^-$. Let us introduce a constant forcing term F in the equation for x: $\dot{x}_k = \alpha(y_k - f(x_k)) + F$. By choosing $F < F_{\rm cr}$, where $F_{\rm cr} \approx 0.6$, the trajectory will settle down to a new equilibrium point which is in the basin $\mathcal{B}(\mathbf{P}^-)$ of the original (unforced) cell. By choosing $F > F_{\rm cr}$, however, only one equilibrium point $\mathbf{P}$ exists, which is in basin $\mathcal{B}(\mathbf{P}^+)$ of the original (unforced) cell. Hence by forcing the cell for an appropriate time interval with $F > F_{\rm cr}$ it is possible to trigger the cell from $\mathbf{P}^-$ to $\mathbf{P}^+$. On the other hand, if the initial state is in $\mathbf{P}^+$, much larger F ($|F| > 0.9$) is needed to trigger back to $\mathbf{P}^-$.

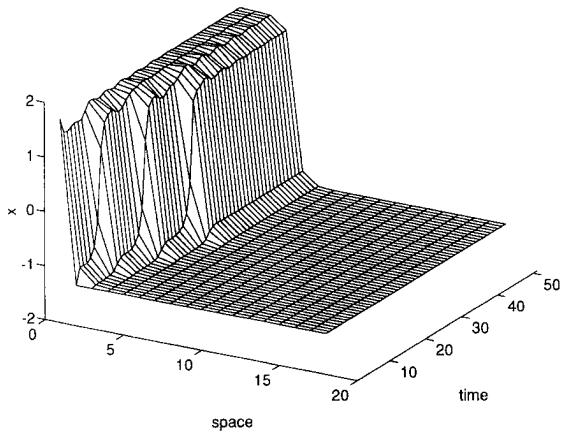

Fig. 4. Propagation failure for diffusion coefficient $D = 0.2795$. The wavefront propagates until it reaches cell 6; the higher-numbered cells remain at equilibrium $\mathbf{P}^-$.

Now let us have a look at the behavior in the whole chain. For large values of D (say, $D > 0.4$), the system exhibits only two attractors: $\{\mathbf{P}^+\} \equiv \{\mathbf{P}_1^+, \cdots, \mathbf{P}_\ell^+\}$ and $\{\mathbf{P}^-\} \equiv \{\mathbf{P}_1^-, \cdots, \mathbf{P}_\ell^-\}$, where $\mathbf{P}_i^\pm \equiv \mathbf{P}^\pm$ for cell number i, with the corresponding basins $\mathcal{B}(\{\mathbf{P}^-\})$ and $\mathcal{B}(\{\mathbf{P}^+\})$. In analogy with the single-cell case, basin $\mathcal{B}(\{\mathbf{P}^+\})$ is larger than $\mathcal{B}(\{\mathbf{P}^-\})$, $\mathcal{B}(\{\mathbf{P}^+\})$ being the "product" of large basins $\mathcal{B}(\mathbf{P}_i^+)$. Therefore, by perturbing the initial condition $\{\mathbf{P}_1^-, \mathbf{P}_2^- \cdots, \mathbf{P}_l^-\}$ to $\{\mathbf{P}_1^+, \mathbf{P}_2^- \cdots, \mathbf{P}_\ell^-\}$, the perturbed point will be already in the basin $\mathcal{B}(\{\mathbf{P}^+\})$ and the trajectory will settle down to $\{\mathbf{P}^+\}$. Fig. 2 gives the global view of the transient shown as a traveling wave front.

From a local point of view, a switching process takes place as follows: the term $D(x_{k-1} - 2x_k + x_{k+1})$ in (1) acts as a feedback and forcing term for cell k. The time waveform of this term (Fig. 3) represents a pulse with above-threshold value and causes the cell to switch from $\mathbf{P}_k^-$ to $\mathbf{P}_k^+$. A series of such triggering processes occur, shifted in time, until all cells have switched to $\mathbf{P}^+$.

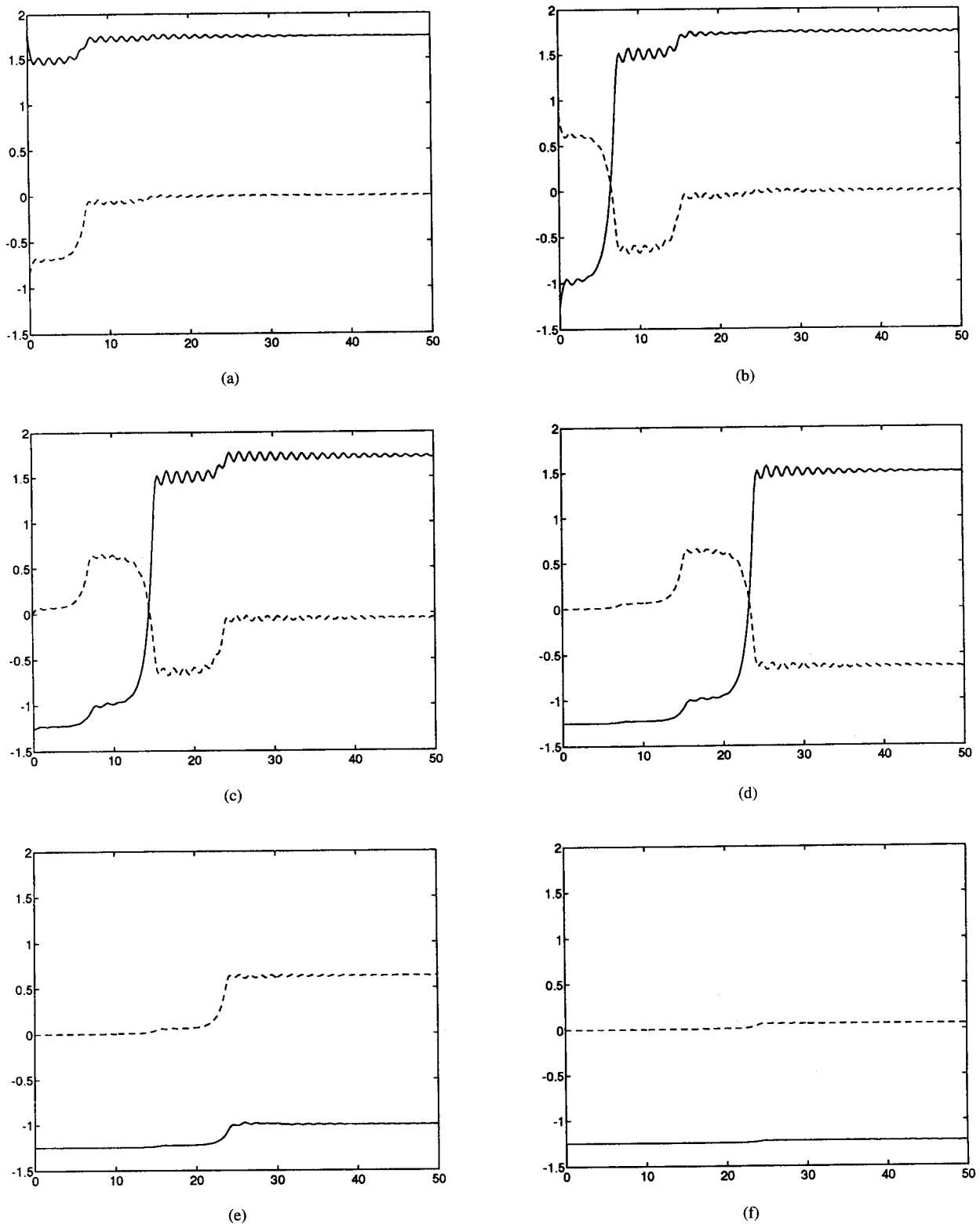

Fig. 5. Time waveforms for propagation failure. Waveforms of the diffusion term $D(x_{k-1} - 2x_k + x_{k+1})$ (dashed line) and variable x (solid line) in cells 1–6 ((a)–(f)).

A different scenario can be observed with values of D below the critical value $D_{cr} \approx 0.2795$. New attractors appear in addition to $\{\mathbf{P}^+\}$ and $\{\mathbf{P}^-\}$, making it possible for the chain to settle down to patterns different from the trivial ones. This is similar to Turing pattern phenomenon in two-grid arrays [16]; however, here only one grid of resistive couplings and diffusion coefficients is involved. Such patterns occur in connection with so-called propagation failure (Fig. 4). The local behavior of the related triggering processes is illustrated by Fig. 5 where the initial condition is $\{\mathbf{P}_1^+, \mathbf{P}_2^- \cdots, \mathbf{P}_\ell^-\}$.

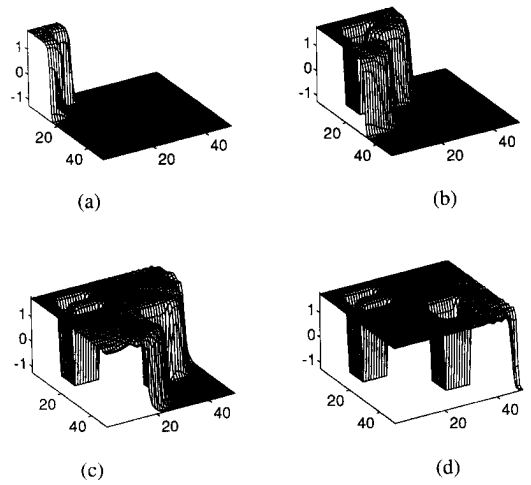

Fig. 6. Traveling wavefront in a 48 × 48 array of Chua's circuits. The snapshots were taken at (a) $t = 32$, (b) $t = 64$, (c) $t = 96$ and (d) $t = 128$. The obstacles were created by keeping some cells clamped at equilibrium $\mathbf{P}^-$ during the simulation.

The first cell is set to equilibrium $\mathbf{P}^+$, so there is no switching [Fig. 5(a)]. In Fig. 5(b), the above-threshold forcing term (dashed line) causes the x variable to rise sharply. This in turn causes a decrease in forcing, but is not sufficient to pull the trajectory back to $\mathbf{P}^-$. A time-shifted version of this process occurs in the third cell (Fig. 5(c)). In cell 4 (Fig. 5(d)), the forcing is still strong enough to trigger the cell, however, it remains locked at a constant value < -0.5, and the cell will go to an equilibrium in $\mathcal{B}(\mathbf{P}^+)$ but different from $\mathbf{P}^+$. Due to further dissipation, the forcing term in cell 5 stays at a subthreshold value and there is no switching (the equilibrium is in $\mathcal{B}(\mathbf{P}^-)$, [see Fig. 5(e)]. The rest of the cells [Figs. 4 and 5(f)], beginning with cell 6, remain virtually unchanged.

B. Traveling Waves in Two-Dimensional Arrays

Two-dimensional CNNs have been found to be capable of modeling parallel processing and image processing [13]. For a demonstration we use a 2-D grid of resistively coupled Chua's circuits. Such arrays can be described by the system

$$\begin{aligned}\dot{x}_{i,j} &= \alpha(y_{i,j} - f(x_{i,j})) \\ &\quad + D(x_{i+1,j} + x_{i-1,j} + x_{i,j+1} + x_{i,j-1} - 4x_{i,j}) \\ \dot{y}_{i,j} &= x_{i,j} - y_{i,j} + z_{i,j} \quad (i,j = 1,2\cdots,l) \\ \dot{z}_{i,j} &= -\beta y_{i,j}. \end{aligned} \tag{4}$$

We use parameter values (3) along with zero-flux boundary conditions and $D = 0.5$ to integrate this system. Fig. 6 shows several snapshots of the traveling wave propagating through a simple image. Since traveling waves do not reflect from obstacles and do not interfere upon collision, the wave bypasses the closed obstacle but fills in the open one. The interior of the closed obstacle remains in the initial state $\mathbf{P}^-$, thus making it possible to distinguish between the two obstacles. Another application of the traveling wave is finding the shortest path in a flat or wrinkled labyrinth [13].

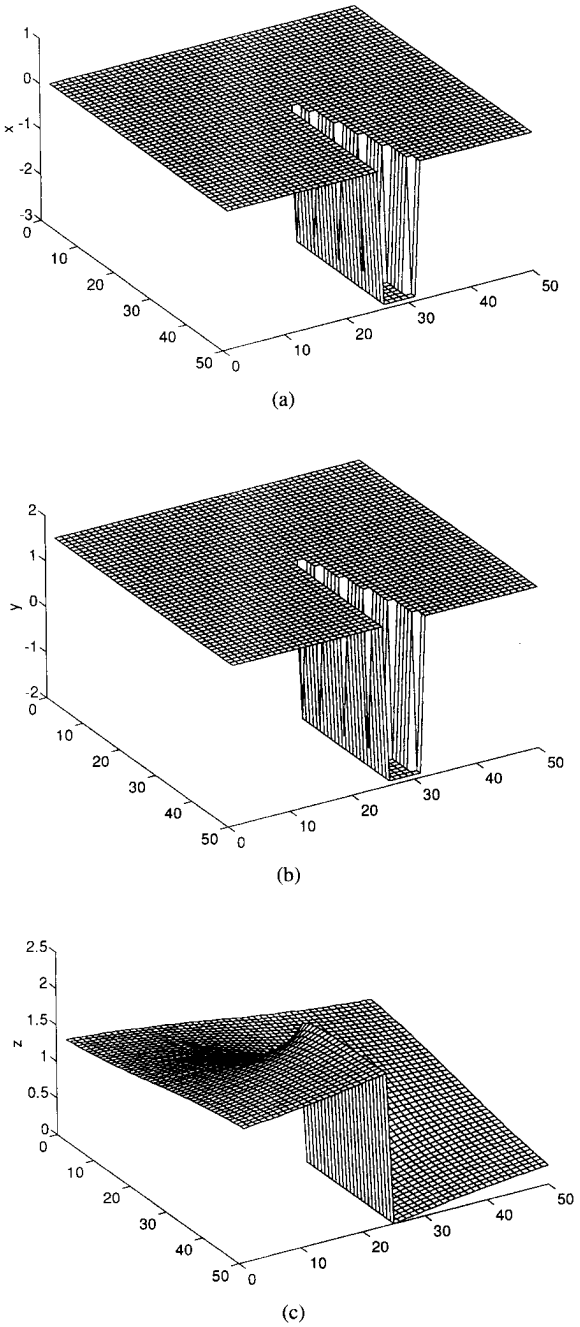

Fig. 7. Initial conditions for spiral formation: (a) variable x, (b) variable y, (c) variable z.

III. Spiral Wave Phenomenon

Spirals are among the most frequently observed structures in the universe, from the microscopic formations in chemical reactions, through large atmospheric formations, up to gigantic clusters of galaxies. The appearance of rotating spiral waves has been studied extensively for several decades, especially in chemical and biological processes, including those in the cardiac muscle [1], retinae [10], and chemical oscillators such as the Belousov–Zhabotinskii reaction [2]. Most of these systems have been successfully modeled by continuous models via partial differential equations. However, the above phenomena can be reproduced more efficiently by using CNNs of discrete, coupled cells [14].

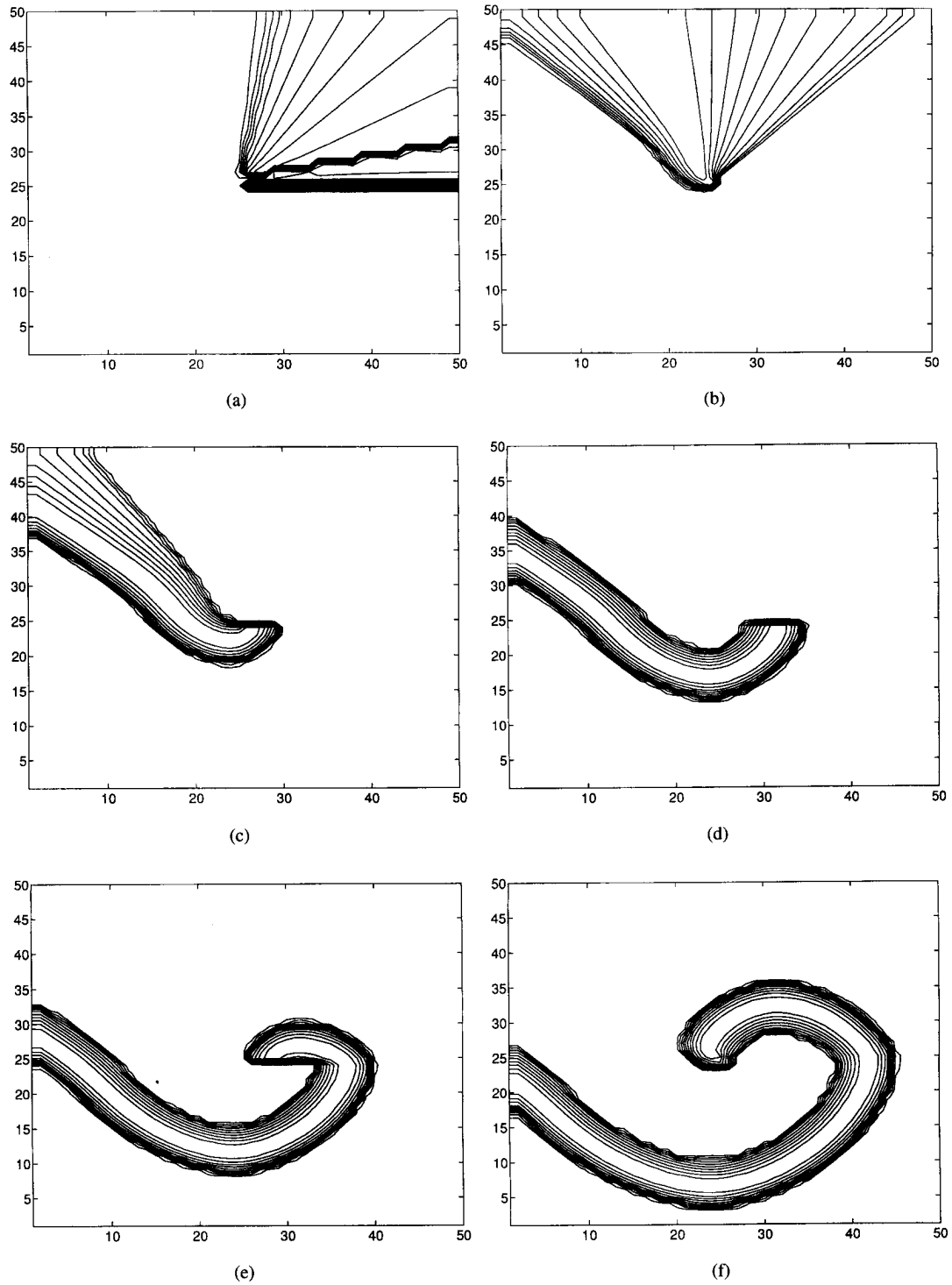

Fig. 8. Contour diagram of spiral development (variable x), with $D = 0.1$ in a 48 × 48 array of Chua's circuits. Snapshots are at time $t = 5$, 10, 15, 20, 25, 30, 35, 40, 45, and 150 [(a) through (j)]. The corresponding 3-D figures are shown in (k) through (t).

In this section we will describe initial conditions for the generation of spiral waves in 2-D arrays of Chua's circuits. In order to give the reader an intuitive idea of local behaviors we plot the waveforms, generated by cells in different sites of the arrays.

We consider both excitable and fluctuating media to generate spiral waves. A detailed treatment of the spiral wave phenomenon in arrays of coupled chaotic Rössler oscillators is given in [6].

A. Spiral Waves in Excitable Media

For the purpose of generating the spiral wave we again consider the nonlinear system (4). With the parameter values

$$\alpha = 10, \quad \beta = 0.3014987, \quad s_1 = 0.078573,$$
$$s_2 = 55, \quad s_0 = -1.25719, \quad \epsilon = 0 \tag{5}$$

and breakpoints $B_1 = -1$, $B_2 = 0.023744$, each individual cell is bistable with the stable equilibrium points $\mathbf{P}^- =$

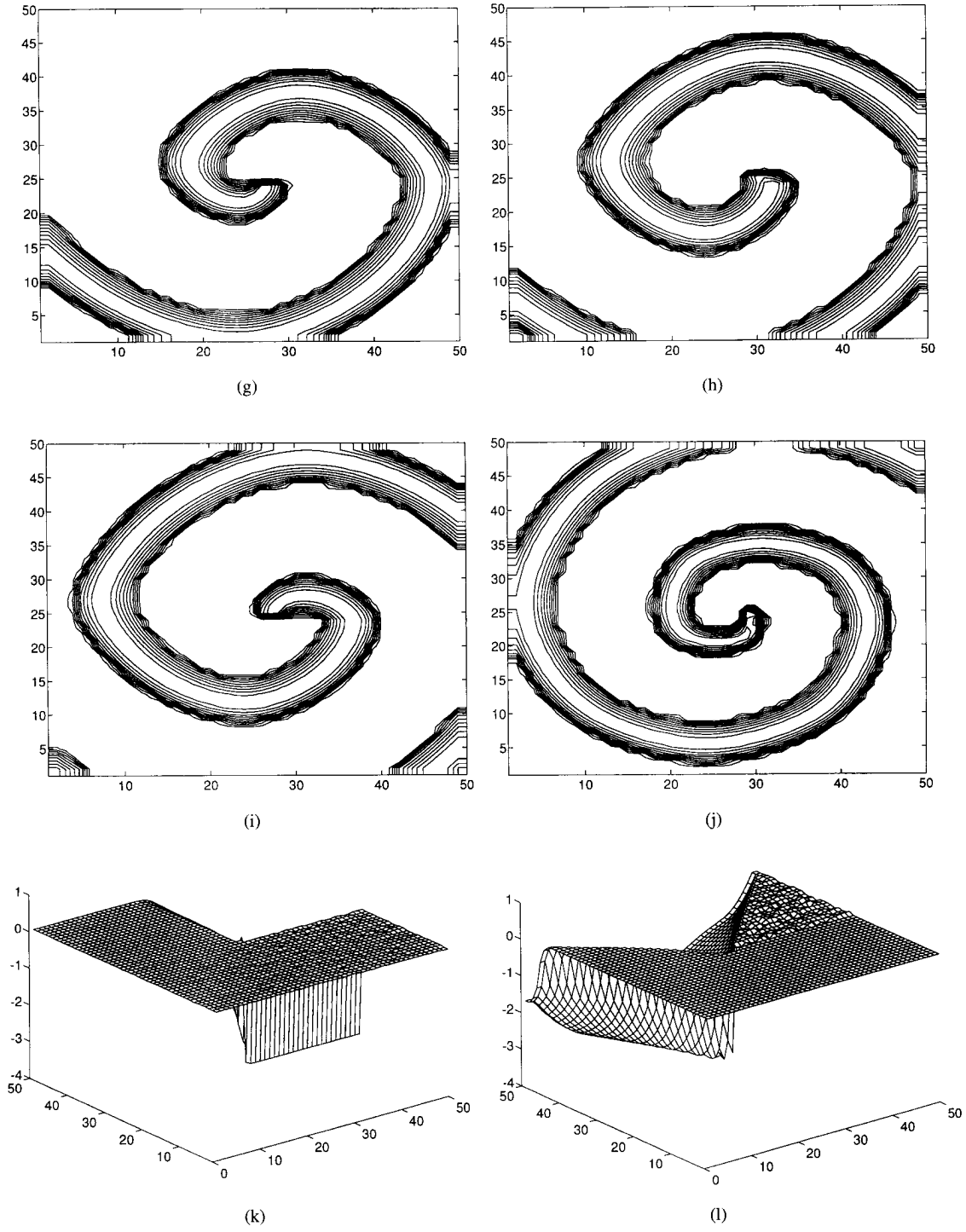

Fig. 8. *(Continued.)*

$[-1.238, 0, 1.238]$, $\mathbf{P}^+ = [0.02385, 0, -0.02385]$. Of these two equilibria, point $\mathbf{P}^-$ is not significant for the dynamics, since its basin is very small compared to that of $\mathbf{P}^+$ which represents the rest state of the excitable cell. We use the set of initial conditions similar to those in [4] and [14], with all the cells in the rest state except for a wedge-like front of excited cells in the x and y variables, and a smoothly declining circular gradient for the z variable (Fig. 7). The C-code fragment shown at the bottom of page 645 can be used to obtain the initial conditions.

Here the variable neq denotes the array size. Several snapshots of the time evolution of the pattern, from its early stages to a fully developed spiral, are shown in Fig. 8. After that the spiral will rotate indefinitely without changing its structure which means it represents a steady state (periodic attractor). The spiral shape is sustained by asynchronous oscillations of individual cells. Some typical features of individual waveforms during spiral motion are depicted in Fig. 9. Each cell operates on an orbit whose phase is site-dependent. While the majority of cells exhibit approximately the same amplitudes and periods

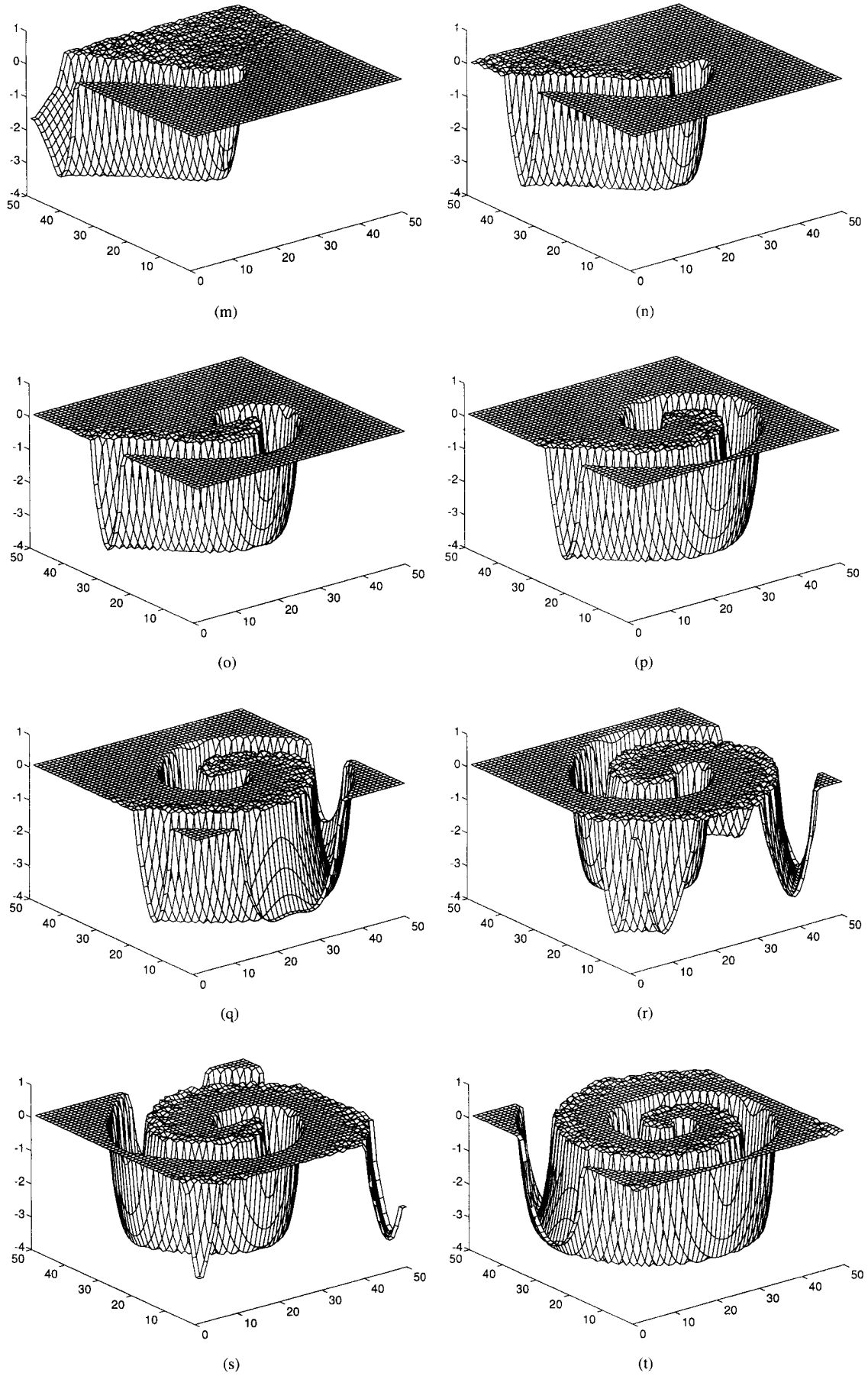

Fig. 8. *(Continued.)*

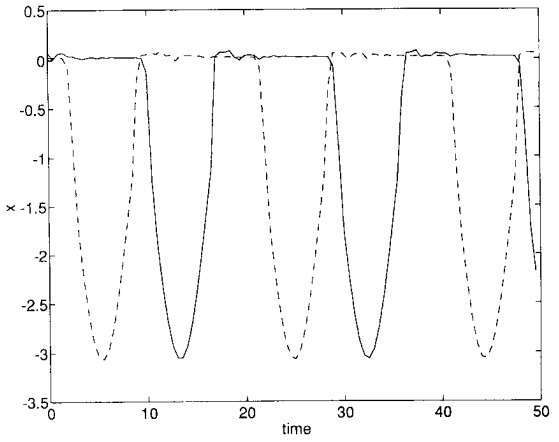

(a)

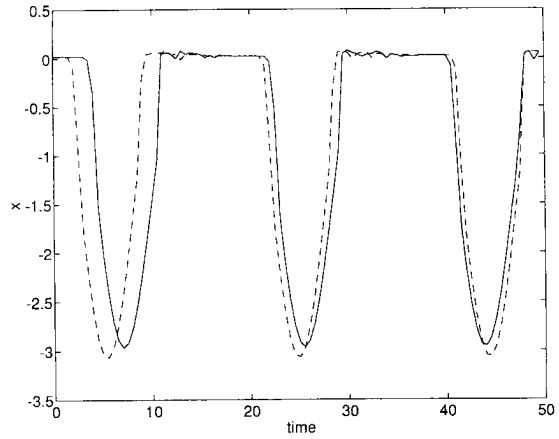

(b)

Fig. 9. Waveforms of variable x from different sites of the array. (a) Cells (25, 38) (solid line) and (25, 48) (dashed line). The waveforms have aproximately the same amplitude and period, but are phase-shifted. (b) Cells (25, 27) (solid line) and (25, 48) (dashed line). The cells near the spiral core exhibit smaller amplitudes and periods.

of variable waveforms, the cells near the spiral center, also called the core of the spiral, have both smaller amplitudes and shorter periods (Fig. 10). The relative phase shift of cells can

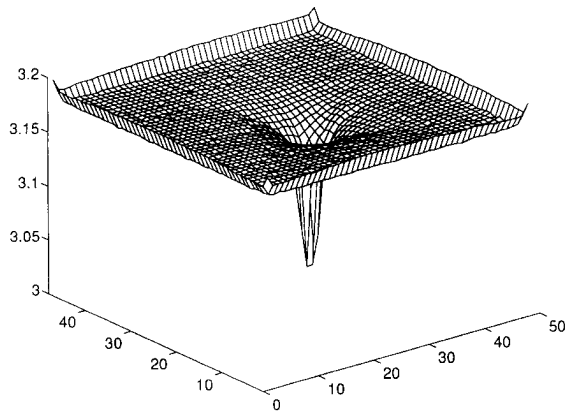

Fig. 10. Amplitude diagram of the x variable. The vertical axis represents the difference between the maximum and minimum values of variable x over several periods of the motion.

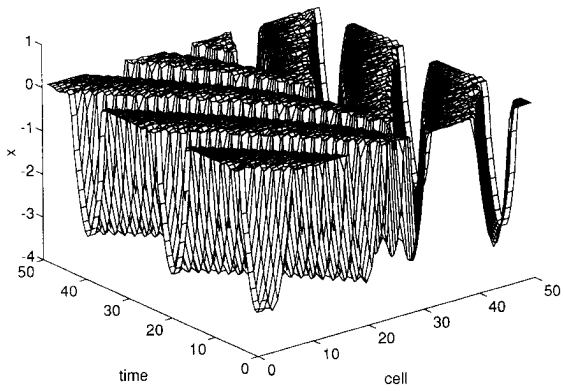

Fig. 11. Phase shift in time waveforms of the x variable for cells (25,i) ($i = 1, 2, \cdots, 48$).

be seen in Fig. 11 where a cumulative plot is given of the waveforms of cells in the center line across the core.

One might ask what the minimum size of an array is for a spiral to develop. While spirals obviously cannot develop in very small arrays, a rotating stable motion can be generated in arrays as small as 4 × 4 cells (see Fig. 12). Such a motion is just a part of the core for a regular spiral in larger arrays.

```
x11 = 0.02 ; y11 = 1.52 ; x22 = -2.9 ; y22 = -1.9 ;
zp = 2.1 ; zm = 0.0 ; lw = 5.0 ; i0 = neq/2 ; j0 = neq/2 ;
for (i=1; i <= neq ; i++)
      for (k=1; k <= neq ; k++)
      {x[i][k] = x11 ; y[i][k] = y11 ; }
for (j=j0+1; j <= neq ; j++)
      for (i=i0+1; i <= i0+1 + (j-j0+1)/lw ; i++)
            {x[i][j] = x22 ; y[i][j] = y22 ; }
for (i=1; i <= neq ; i++)
      for (j=1; j <= neq ; j++)
      { aux1 = sqrt((i-i0)*(i-i0)+(j-j0)*(j-j0)) ; aux2 = 2*3.14159 ;
      if (i==i0 &&j != j0) z[i][j] = (zp/aux2)*acos((j-j0)/aux1) ;
      if (i>i0 ) z[i][j] = (zp/aux2)*acos((j-j0)/aux1);
      if (i<i0) z[i][j] = (zp/aux2)*(aux2 - acos((j-j0)/aux1)) ;
      }
      z[i0][j0] = zp/2 ;
```

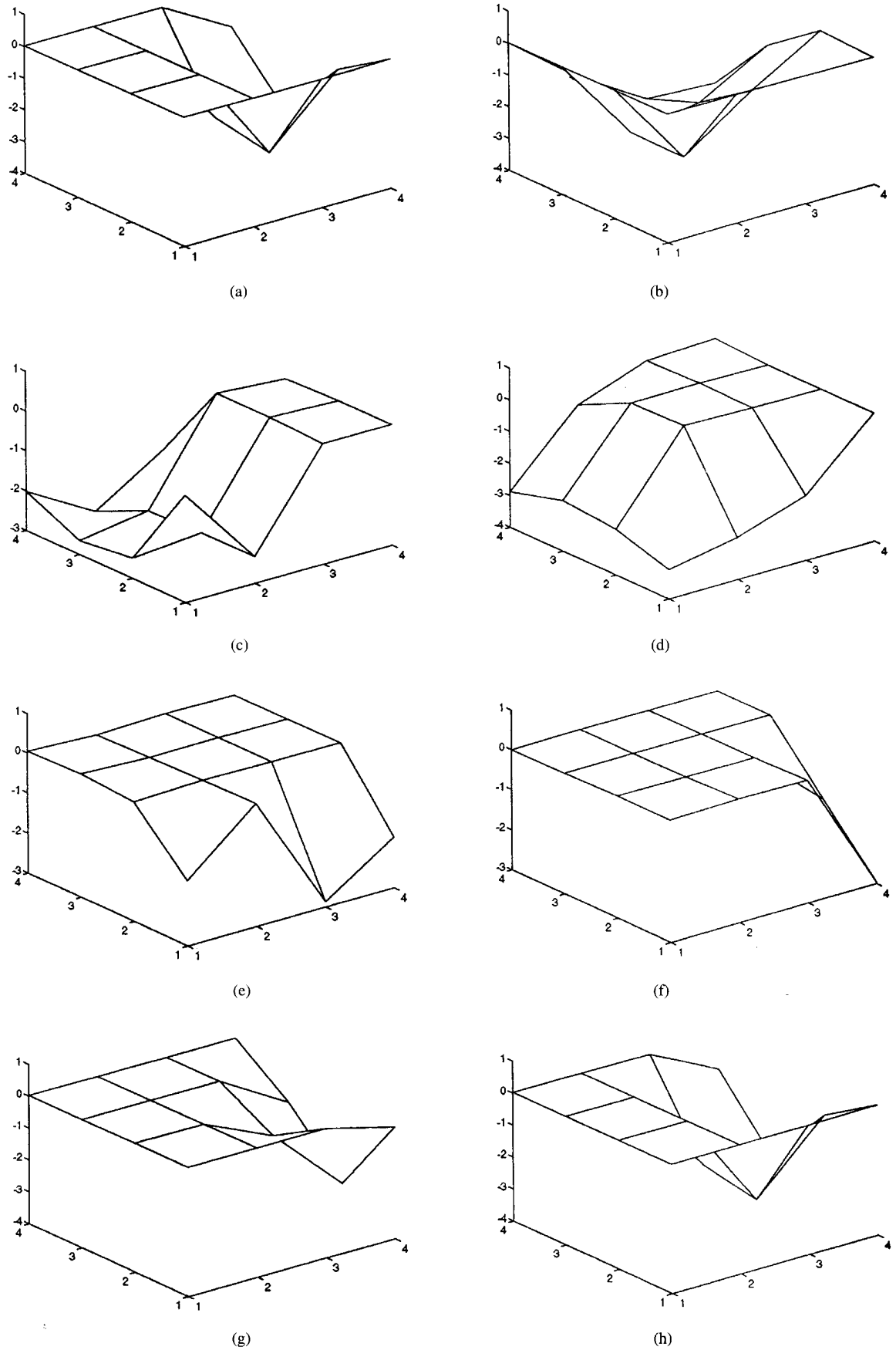

Fig. 12. Rotating stable motion (variable x) in a $4\times$ 4 array of excitable Chua's circuits. The snapshots were taken from a period of 24 time units. The diffusion coefficient was $D = 0.02$, parameter values as in Figs. 7–9 and the initial conditions were generated with the same procedure.

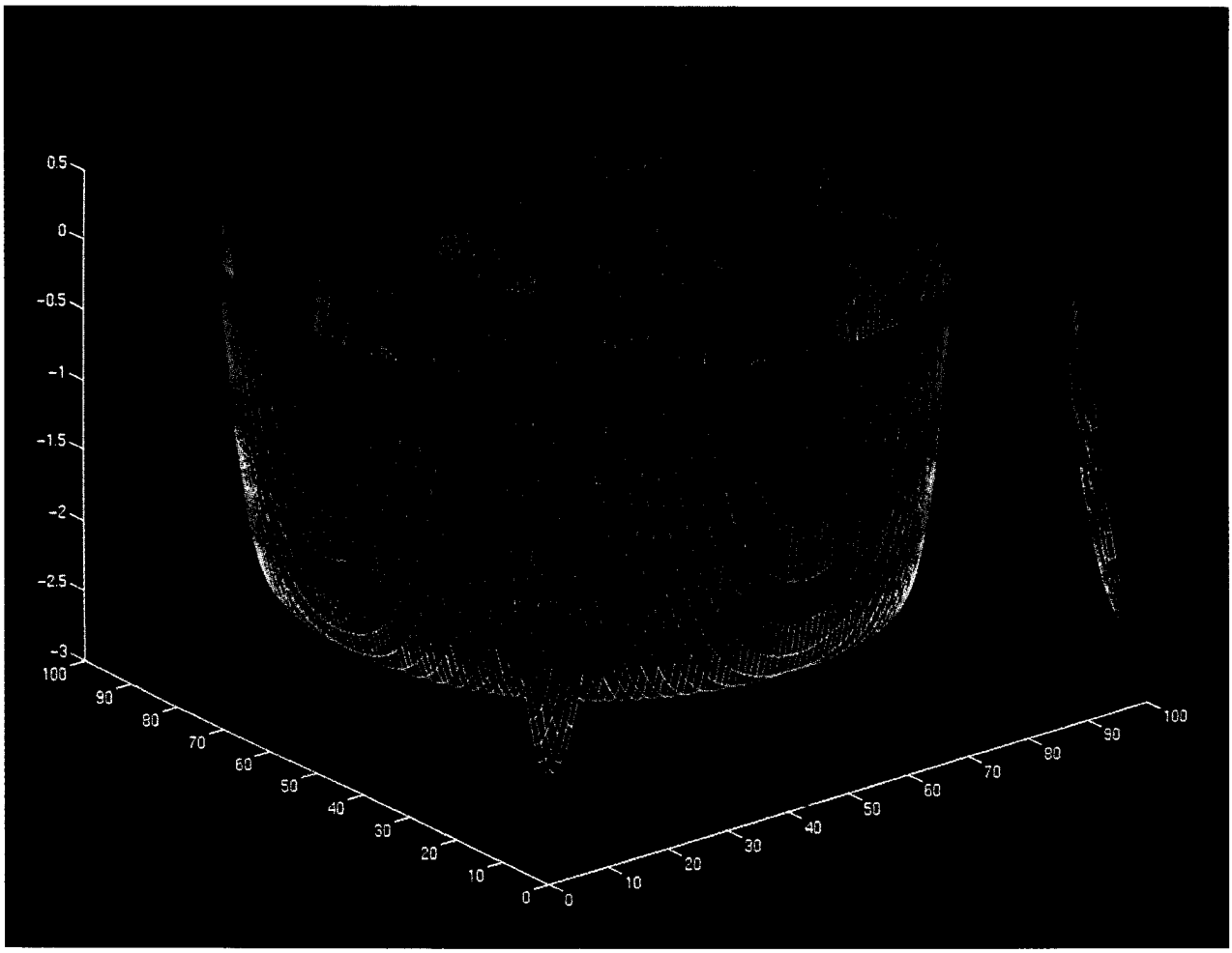

Fig. 13. A fully developed spiral in a 98 × 98 array of Chua's circuits (fluctuating medium, corresponding to $D = 5$).

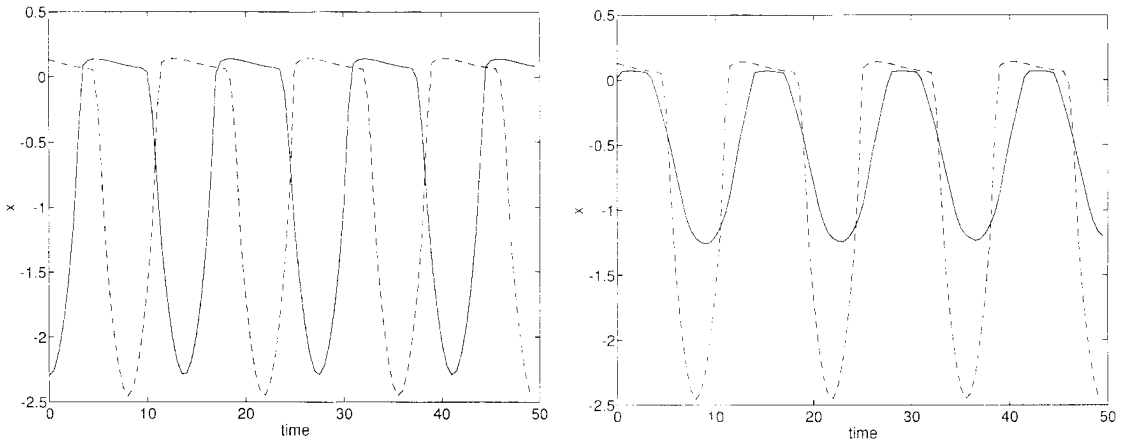

Fig. 14. Time waveforms of variable x from different sites of 2-D fluctuating medium with diffusion coefficient $D = 5$. (a) Cells (25, 15) (solid line) and (25, 48) (dashed line). (b) Cells (25, 29) (solid line) and (25, 48) (dashed line). The cells near the spiral core exhibit smaller amplitudes but approximately the same periods (compare Fig. 9).

B. Spiral Waves in Fluctuating Media

By using modified parameters

$$\alpha = 10, \quad \beta = 0.334091, \quad s_1 = 0.020706,$$
$$s_2 = 15, \quad s_0 = -0.921, \quad \epsilon = 0 \tag{6}$$

and breakpoints $B_1 = -1$, $B_2 = 0.0591486$, we obtain a medium in which uncoupled cells operate in a periodic regime. Due to the high relaxational character of the cell motions, such media are capable of supporting spiral waves (Fig. 13). One can use the same initial conditions as with excitable

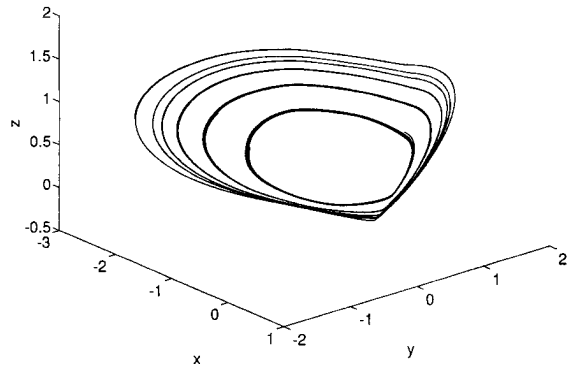

Fig. 15. State-space trajectories corresponding to cells (25, 15), (25, 25), (25, 26), (25, 27), (25, 28) and (25, 29) (largest to smallest).

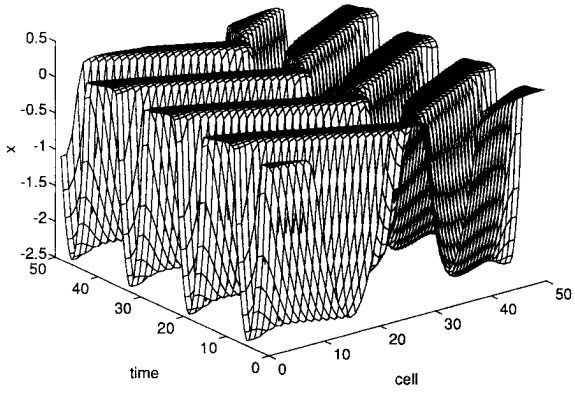

Fig. 16. Phase shift pattern in the time waveforms of the x variable for cells $(25, i)(i = 1, 2, \cdots, 48)$ in a fluctuating medium composed of 48 × 48 Chua's circuits.

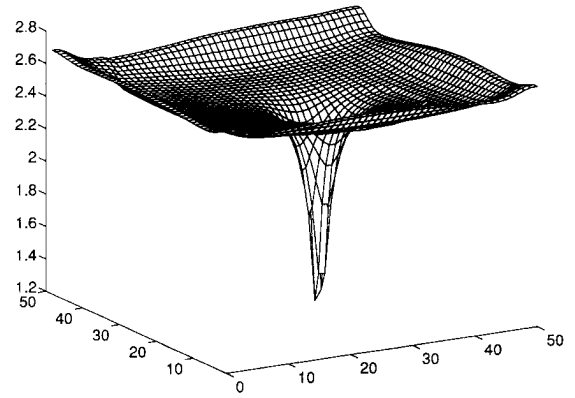

Fig. 17. Amplitude diagram of the x variable analogous to Fig. 10. Parameter values (6) and diffusion coefficient $D = 5$ were used.

media. The process of spiral development is similar to Fig. 8, however, in this case the behavior at the spiral core seems to be more differentiated from the rest of the cells. The waveform amplitudes of core cells are much smaller (Figs. 14 and 15). On the other hand, the periods are approximately the same, in contrast to Fig. 9(b). A phase shift pattern similar to Fig. 11 is observed in fluctuating media (Fig. 16). In Fig. 17 we plot the amplitudes for individual cells, analogously to Fig. 10. The amplitudes for core cells are much smaller than in the excitable medium.

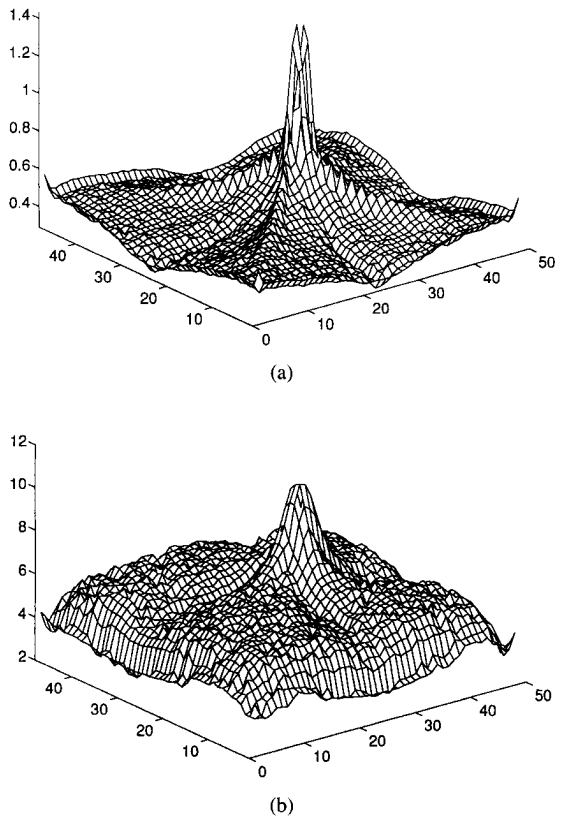

Fig. 18. Amplitude diagrams for the diffusion term. (a) Excitable medium [$D = 0.1$ and parameter values (5)]. (b) Fluctuating medium [$D = 5$ and parameter values (6)].

By plotting the amplitudes of the diffusion term $D(x_{i,j+1} + x_{i,j-1} + x_{i-1,j} + x_{i+1,j} - 4x_{i,j})$ we observe a phenomenon opposite to Figs. 10 and 17: while the amplitudes of individual cells at the core are small, in the diffusion term they sum up to larger values than outside the core. In other words, the cells at the core are subject to stronger forcing than the rest of array cells (Fig. 18).

REFERENCES

[1] M. A. Allesie, F. I. M. Bonke, and T. Y. G. Schopman, "Circus movement in rabbit atrial muscle as a mechanism in tachycardia," *Circulation Res.*, vol. 33, pp. 54–62, 1973.

[2] S. C. Müller, T. Plesser, and B. Hess, "Two-dimensional spectrophotometry of spiral wave propagation in the Belousov-Zhabotinskii reaction I. Experiments and digital representation. II. Geometric and kinematic parameters," *Physica*, vol. D24, pp. 71–96, 1987.

[3] A. T. Winfree, "Scroll-shaped waves of chemical activity in three dimensions," *Science*, vol. 181, pp. 937–939, 1973.

[4] W. Jahnke and A. T. Winfree, "A survey of spiral-wave behaviors in the Oregonator model," *Int. J. Bifurc. and Chaos*, vol. 1, no. 2, pp. 445–466, 1991.

[5] A. M. Pertsov, E. A. Ermakova, and A. V. Panfilov, "Rotating spiral waves in a modified Fitzhugh–Nagumo model," *Physica*, vol. 14D, pp. 117–124, 1984.

[6] R. R. Klevecz, J. Bolen, and O. Durán, "Self-organization in biological tissues: Analysis of asynchronous and synchronous periodicity, turbulence and synchronous chaos emergent in coupled chaotic arrays," *Int. J. Bifurc. and Chaos*, vol. 2, no. 4, pp. 941–953, 1992.

[7] R. N. Madan, Ed., *Chua's Circuit: A Paradigm for Chaos*. Singapore: World Scientific, 1993.

[8] M. Dolnik and M. Marek, "Extinction of oscillations in forced and coupled reaction cells," *J. Phys. Chem.*, vol. 92, pp. 2452–2455, 1988.

[9] A. C. Scott, "The electrophysics of a nerve fiber," *Rev. Mod. Phys.*, vol. 47, pp. 487–533, 1975.

[10] J. Bures, V. I. Koroleva, and N. A. Gorelova, "Leao's spreading depression, an example of diffusion-mediated propagation of excitation

in the central nervous system," in *Autowaves and Structures Far from Equilibrium*, V. I. Krinsky, Ed. New York: Springer-Verlag, 1984, pp. 180–183.

[11] J. P. Keener, "Propagation and its failure in coupled systems of discrete excitable cells," *SIAM J. Appl. Math.*, vol. 47, pp. 556–572, 1987.

[12] V. Pérez-Muñuzuri, V. Pérez-Villar, and L. O. Chua, "Traveling wave front and its failure in a one-dimensional array of Chua's circuits," *J. Circuits, Syst., and Comput.*, vol. 3, no. 1, pp. 211–215, 1993.

[13] ——, "Autowaves for image processing on a two-dimensional CNN array of excitable nonlinear circuits: flat and wrinkled labyrinths," *IEEE Trans. Circuits Syst.*, vol. 40, no. 3, pp. 174–181, 1993.

[14] A. Pérez-Muñuzuri, V. Pérez-Muñuzuri, V. Pérez-Villar, and L. O. Chua, "Spiral waves on a two-dimensional array of nonlinear circuits," *IEEE Trans. Circuits Syst.*, vol. 40, no. 11, pp. 872-877, 1993.

[15] V. Špány and L. Pivka, "Boundary surfaces in sequential circuits," *Int. J. Circuit Theory Applicat.*, vol. 18, pp. 349–360, 1990.

[16] L. Goraş *et al.*, "Turing patterns in CNNs—Parts I, II, III," *IEEE Trans. Circuits Syst.*, vol. 42, no. 10, pp. 602–637, this issue.

Ladislav Pivka, for a photograph and biography, see this issue, p. 637.